

# Information-Assisted Carnot Engine Surpasses Standard Thermodynamic Bounds

Yang Xiao<sup>1</sup>, Qian Zeng<sup>2</sup>, and Jin Wang<sup>3\*</sup>

<sup>1</sup> College of Physics, Jilin University, Changchun 130022, China

<sup>2</sup> State Key Laboratory of Electroanalytical Chemistry,

Changchun Institute of Applied Chemistry, Changchun, Jilin 130022, China

<sup>3</sup> Department of Chemistry and Department of Physics and Astronomy,

State University of New York at Stony Brook, Stony Brook, New York 11794, USA

(Dated: July 21, 2025)

Information can improve heat engine performance, but the underlying principles are still not so clear. Here we introduce a Carnot information machine (CIE) and obtain a quantitative relationship between the engine performance and information. We demonstrate that the presence of information changes allows the CIE to operate as a heat engine in the regime where the standard Carnot cycle is prohibited, ensures that the efficiency of the CIE is greater than or equal to the standard Carnot efficiency, and significantly enables it to achieve 100% efficiency with positive work extraction for arbitrary two-level systems. We explicitly demonstrate these features using a spin-1/2 system and propose an experimental implementation scheme based on a trapped  $^{40}\text{Ca}^+$  ion.

*Introduction.*—The information engine, which utilizes information to extract work from heat reservoirs [1–20], was first conceptualized by Szilard [1] as a solution to Maxwell’s demon paradox [21, 22]. Far from being merely a theoretical construct, such information engines represent fundamental mechanisms widespread in nature [23–27]. Among these, measurement-feedback engines, also known as Maxwell’s demon-like mechanisms, are particularly significant. In these engines, the demon controls the working system’s evolution based on information stored in its memory [2, 9–16], a process that has profoundly influenced the development of modern thermodynamics [2, 28–32]. These naturally occurring mechanisms have been extensively studied and experimentally realized across various physical systems, including spin-boson [13], Brownian motion [33–36], electronic [14, 15, 37, 38], photonic [39], and superconducting circuits system [40].

Conventional heat engines operating between thermal reservoirs at inverse temperatures  $\beta_h$  and  $\beta_c$  ( $\beta_c > \beta_h$ ) convert thermal energy into mechanical work and its efficiency is fundamentally limited by the Carnot efficiency  $\eta_C = 1 - \beta_h/\beta_c$  [41, 42]. Although information-assisted cycles can enable efficiencies beyond this limit [29, 43, 44], the mechanism by which information achieves this remains elusive. The critical challenge lies in the lack of a quantitative relationship between information and heat engine performance (output work and efficiency). The key to achieving this hinges on simultaneously regulating heat engine performance and mutual information.

To address these crucial challenges, we propose a Carnot information engine (CIE), incorporating an imperfect classical measurement and feedback control into the standard Carnot cycle. Our analytical framework establishes explicit relations between mutual information changes and work output as well as efficiency. Specifi-

cally, our theoretical analysis demonstrates that: (i) information changes enable the CIE to operate as a heat engine in regimes where the standard Carnot cycle is forbidden, which is achieved through entropy flow compensation via measurement and feedback; (ii) information changes make the efficiency of the CIE be greater than or equal to the standard Carnot efficiency; and (iii) most significantly, the CIE can achieve 100% efficiency while producing positive work, breaking the efficiency limits of conventional heat engines. To validate these theoretical findings, we illustrate our results with a detailed example of a spin-1/2 CIE and present an experimental implementation scheme based on a trapped  $^{40}\text{Ca}^+$  ion.

*Carnot information engine cycle.*— In this heat engine, the working system’s energy levels are characterized by the populations in excited and ground states, denoted by  $n_e$ , and  $n_g$ , respectively, with corresponding energy levels defined as  $\varepsilon^e = \omega n_e$ ,  $\varepsilon^g = \omega n_g$ , where  $\omega$  represents the system’s frequency. Let  $x$  denote the system state. When the system reaches thermal equilibrium with a heat reservoir at inverse temperature  $\beta$ , the occupation probabilities of the excited and ground states are determined as  $P^e = P(x = e) = \exp(-\beta\varepsilon^e)/Z$  and  $P^g = P(x = g) = \exp(-\beta\varepsilon^g)/Z$  respectively, where  $Z = \exp(-\beta\varepsilon^e) + \exp(-\beta\varepsilon^g)$  is the partition function.

The CIE operates through five distinct strokes, as illustrated in Fig. 1(a): two standard Carnot cycle strokes (adiabatic compression stroke  $A \rightarrow B$  and isothermal expansion stroke  $B \rightarrow C$ ), followed by three control strokes  $C \rightarrow C' \rightarrow D' \rightarrow A$ . During the adiabatic compression stroke  $A \rightarrow B$ , the system undergoes a compression from  $\omega_A$  to  $\omega_B$  while maintaining constant population numbers. In the subsequent isothermal expansion stroke  $B \rightarrow C$ , the system interacts with the hot reservoir at inverse temperature  $\beta_h$ , the system frequency decreases reversibly from  $\omega_B$  to  $\omega_C$ . This process results in heat absorption by the system be proportional to the temperature times the entropy change [45]

$$Q_h = \beta_h^{-1}(S_C - S_B), \quad (1)$$

\*Electronic address: [jin.wang.1@stonybrook.edu](mailto:jin.wang.1@stonybrook.edu)

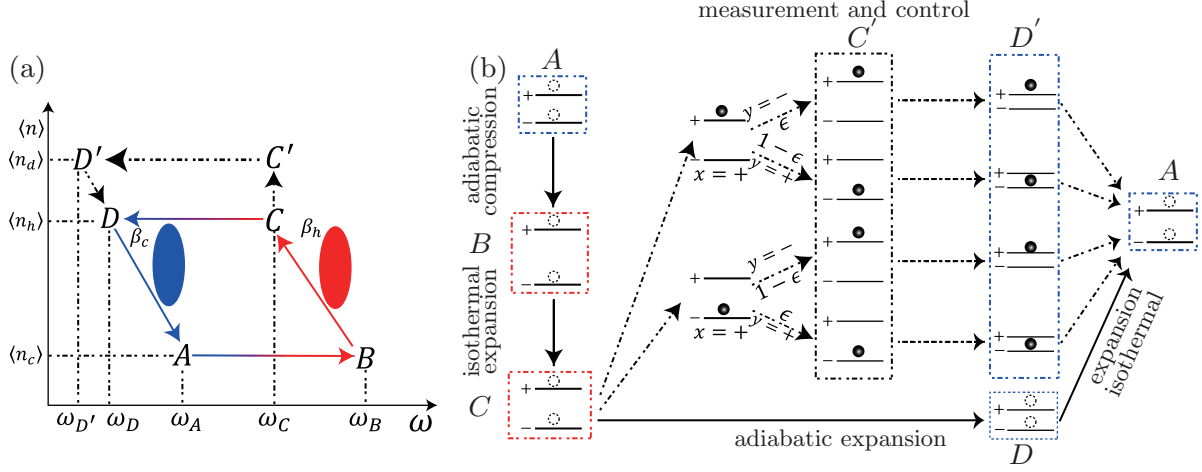


FIG. 1: Schematic of the CIE. (a) The average population-frequency diagram for an arbitrary two-level work system. The standard Carnot cycle consists of four consecutive strokes: adiabatic compression  $A \rightarrow B$ , isothermal expansion  $B \rightarrow C$ , adiabatic expansion  $C \rightarrow D$ , isothermal compression  $D \rightarrow A$ . The CIE contains five consecutive strokes: adiabatic compression  $A \rightarrow B$ , isothermal expansion  $B \rightarrow C$ , measurement and control  $C \rightarrow C'$ , adiabatic expansion  $C' \rightarrow D'$ , and isothermal compression  $D' \rightarrow A$ . (b) Explicit realization of the spin-1/2 CIE. The solid (dashed) arrows represent the standard Carnot cycle (CIE) and the solid (dashed) balls represent the system state being known (unknown)

where,  $S_B = S_A = S_c = -P_A^e \ln P_A^e - P_A^g \ln P_A^g$  and  $S_C = S_h = -P_C^e \ln P_C^e - P_C^g \ln P_C^g$  represent the entropy of the system at points  $B$  and  $C$ .

The remaining three strokes are controlled by the demon through measurement and feedback. At point  $C$ , the demon performs a measurement on the system state  $x_C$  ( $x_C = e, g$ ) with a measurement error characterized by  $p(y \neq x_C | x_C) = \epsilon$ . Here,  $y = e, g$  denotes the measurement outcome. Based on this measurement, the demon implements a state-dependent control protocol. When  $y = g$ , the control protocol consists of three consecutive strokes: (a)  $C \rightarrow C'$ : The system state is maintained unchanged. (b)  $C' \rightarrow D'$ : The system undergoes an adiabatic expansion while keeps constant state. (c)  $D' \rightarrow A$ : The system interacts with the cold reservoir at inverse temperature  $\beta_c$  and returns to its initial state. Alternatively, when  $y = e$ , the demon first flips the system's energy level during  $C \rightarrow C'$ , then performs the same subsequent control sequence as in the  $y = g$  case [46]. The detailed dynamics of these control strokes are explained in the following section.

The first control stroke  $C \rightarrow C'$ : Following the measurement, the system becomes correlated with the demon. The mutual information between them is given by (see Appendix A)

$$I_C = S_Y - S_\epsilon, \quad (2)$$

where  $S_Y = -P_y^g \ln P_y^g - P_y^e \ln P_y^e$  represents the demon's entropy and  $S_\epsilon = -(1 - \epsilon) \ln(1 - \epsilon) - \epsilon \ln \epsilon$  denotes the entropy of the measurement error. Here  $P_y^e = P(y = e) = P_C^e(1 - \epsilon) + P_C^g \epsilon$ , and  $P_y^g = P(y = g) = P_C^e \epsilon + P_C^g(1 - \epsilon)$  represent the probabilities of measurement outcomes  $y = e$  and  $y = g$ , respectively.

Then the demon utilizes the obtained information  $I_C$  to perform work by flipping the system's energy level while fixing the system frequency at  $\omega_C$ . This operation transforms the system's probability distribution to  $P_{C'}^e = P_C^e P(y = g | x_C = e) + P_C^g P(y = e | x_C = g) = \epsilon$  and  $P_{C'}^g = P_C^e P(y = e | x_C = e) + P_C^g P(y = g | x_C = g) = 1 - \epsilon$ , where the system's entropy becomes to the measurement error entropy  $S_\epsilon$ . Through the detailed balance condition  $\exp[\beta_d(\epsilon_C^e - \epsilon_C^g)] = P_{C'}^g / P_{C'}^e$ , the effective inverse temperature  $\beta_d$  after this control stroke can be determined. Based on the distribution  $P_{C'}^e$  and  $P_{C'}^g$ , the work exerted by the demon on the system can be calculated as (see Appendix A)

$$\begin{aligned} W_d &= \sum_{x_C, x_{C'}, y} P(x_C \rightarrow x_{C'} | y) P(y) (\epsilon_C^{x_{C'}} - \epsilon_C^{x_C}) \\ &= \omega_C (\langle n_d \rangle - \langle n_h \rangle), \end{aligned} \quad (3)$$

where  $P(x_C \rightarrow x_{C'} | y)$  is the condition probability for the system's evolutionary trajectory from  $x_C$  to  $x_{C'}$  based on the measurement outcome  $y$ . Due to this control stroke is nondegenerate, this probability is equal to the condition probability  $P(x_C | y)$ . Here  $\langle n_h \rangle = P_C^e n_e + P_C^g n_g$  and  $\langle n_d \rangle = P_{C'}^e n_e + P_{C'}^g n_g$  represent the average populations of the system at points  $C$  and  $C'$ , respectively. After being utilized by the demon, the remaining mutual information at point  $C'$  can be expressed as (see Appendix A)

$$I_{C'} = S_Y - S_h. \quad (4)$$

Then, the information changes during this process are given by  $\Delta I = I_{C'} - I_C = S_\epsilon - S_h$ . This quantity characterizes how the demon modulates the system entropy

through its imperfect measurement and control operations.

The second control stroke  $C' \rightarrow D'$ : during this stroke, the demon fixes the system state at the final state of the conditional trajectory  $x_C \rightarrow x_{C'}|y$ . Simultaneously, the demon guides the system to expand adiabatically from  $\omega_C$  to  $\omega_{D'}$ . This operation indicates the conditional probability  $P(x_C \rightarrow x_{D'}|y) = P(x_C \rightarrow x_{C'}|y) = P(x_{C'}|y)$ . Consequently, the system probability distribution at the point  $D'$  is the same as at point  $C'$ , i.e.,  $P_{x_{D'}=x_{C'}} = P_{x_{C'}}$ . At the end of this stroke, the system reaches thermal equilibrium with the cold reservoir. Through the detailed balance condition  $\exp[\beta_c(\varepsilon_{D'}^e - \varepsilon_{D'}^g)] = P_{D'}^g/P_{D'}^e$ , the system frequency  $\omega_{D'}$  modulated by the demon can be determined.

The third control stroke  $D' \rightarrow A$ : The demon couples the system to the cold reservoir with the inverse temperature  $\beta_c$  while modulating the system frequency from  $\omega_{D'}$  to its initial quantity  $\omega_A$ . Throughout this process, the system maintains equilibrium with the cold reservoir, causing the system's distribution to become independent of the demon's control. The heat absorbed from the cold reservoir can be expressed through the entropy flow from the system to the cold reservoir: [32, 47]

$$\begin{aligned} Q_c^d &= \sum_{x_{D'}, x_A, y} (\beta_c)^{-1} P(x_{D'} \rightarrow x_A | x_{D'}, y) \\ &\times P(x_{D'}|y) P(y) \ln \frac{P(x_A \rightarrow x_{D'} | x_A, y)}{P(x_{D'} \rightarrow x_A | x_{D'}, y)} \\ &= \beta_c^{-1} (S_c - S_\epsilon) = Q_c - \beta_c^{-1} \Delta I, \end{aligned} \quad (5)$$

where  $Q_c = \beta_c^{-1} (S_c - S_h)$  represents the heat absorbed from the cold reservoir during the isothermal compression stroke  $D \rightarrow A$  of the standard Carnot cycle as shown in Fig. 1(a). Note that,  $P(x_{D'} \rightarrow x_A | x_{D'}, y)$  quantifies the condition probability for the system's evolutionary trajectory from  $x_{D'}$  to  $x_A$ , based on the measurement outcome  $y$ . Because the system and the demon's memory become uncorrelated during this stroke, this probability is equal to the initial probability  $P(x_A)$ . Similarly, the probability for time-reversal trajectory  $P(x_A \rightarrow x_{D'} | x_A, y)$  is equal to  $P(x_{D'})$ . The last equality of Eq. (5) allows us to decompose the isothermal compression stroke  $D' \rightarrow A$  into two distinct subsections: the demon-induced compression  $D' \rightarrow D$ , and the standard Carnot compression  $D \rightarrow A$ . In the first subsection, the system releases a net heat  $\Delta I/\beta_c$  into the cold reservoir, which compensates for the demon-induced entropy change during the first control stroke. Thus, the CIE can be regarded as a combination of the standard Carnot cycle  $A \rightarrow B \rightarrow C \rightarrow D \rightarrow A$  and the information-driven cycle  $C \rightarrow C' \rightarrow D' \rightarrow D \rightarrow C$ .

*The performance of the information Carnot engine.*— The net work produced by the information-driven cycle is defined as

$$W_{\text{net}} = W_d - \beta_c^{-1} \Delta I. \quad (6)$$

Combining Eqs. (1), (3), (5), and (6), the total output work produced by the working system's size variation after completing one cycle is given by

$$W_{\text{tot}}^d = W_{\text{tot}} + W_{\text{net}}, \quad (7)$$

where  $W_{\text{tot}} = Q_h + Q_c = (S_h - S_c)(\beta_h^{-1} - \beta_c^{-1})$  quantifies the output work of the standard Carnot cycle. A key observation from Eq. (7) is that when the net work  $W_{\text{net}}$  is positive, the CIE produces greater output work than the standard Carnot engine. Moreover, this reveals the first advantage of the CIE: in the regime  $S_h < S_c < S_\epsilon$  ( $S_c < S_\epsilon$  ensures  $Q_c^d < 0$ ), the operation of the standard Carnot engine as a heat engine is forbidden due to  $Q_c > 0$ ,  $Q_h < 0$ , and  $W_{\text{tot}} < 0$ . However, if the net work satisfies  $W_{\text{net}} > (S_c - S_h)(\beta_h^{-1} - \beta_c^{-1})$ , where the net work generated by information-driven cycle compensates for the negative work produced by the standard Carnot cycle, the CIE can operate as a heat engine because the total work output and the total energy injected into the system which is defined as  $Q_h^d = Q_h + W_d$  of the CIE satisfy  $W_{\text{tot}}^d > 0$  and  $Q_h^d > (S_\epsilon - S_c)\beta_c^{-1} > 0$ .

The efficiency  $\eta_d$  (see Appendix B) of the CIE, combining Eqs. (1), (3), and (7), is given by

$$\eta_d = \frac{W_{\text{tot}}^d}{Q_h^d} = \eta_C + \frac{1}{\beta_c} \frac{\beta_h W_d - \Delta I}{Q_h^d}. \quad (8)$$

Eq. (8) indicates that the condition for the CIE efficiency to defeat the standard Carnot efficiency is that the work performed by the demon on the system surpasses the heat required to flow from the hot reservoir to the system to produce an equivalent entropy change as that generated by the work. In Appendix C, we have proven that  $\beta_h W_d \geq \Delta I \geq \beta_d W_d$ . By incorporating this relationship into Eq. (8), the efficiency bounds can be obtained

$$\eta_C \leq \eta_d \leq \eta_{\text{up}} = \eta_C + \frac{\beta_h \Delta I \Delta T}{\beta_c Q_h^d}, \quad (9)$$

where  $\Delta T = \beta_d^{-1} - \beta_h^{-1}$  denotes the temperature variation of the system, induced by the demon control during the stroke  $C \rightarrow C'$ . The term  $\eta_{\text{up}}$  represents the upper bound of the CIE efficiency and serves, to some extent, as an indicator of the efficiency level. According to the definition of  $\Delta I$ , the information changes increase with the measurement error within the regime  $0 \leq \epsilon \leq 0.5$ . As the measurement error increases, the effective temperature  $\beta_d^{-1}$  also rises, leading to a positive correlation between  $\beta_d^{-1}$  and  $\Delta I$ . When  $\Delta I = 0$ , where  $S_\epsilon = S_h$ , resulting in  $\beta_d^{-1} = \beta_h^{-1}$ . Consequently, if  $\Delta I < 0$ , then  $\Delta T < 0$ ; conversely, if  $\Delta I > 0$ , then  $\Delta T > 0$ . Thus, in the regime  $\Delta I > 0$ ,  $\eta_{\text{up}}$  increases with  $\Delta I$ , while in the regime  $\Delta I < 0$ ,  $\eta_{\text{up}}$  increases as  $\Delta I$  decreases. Furthermore, when  $\Delta I = 0$ , the equation in Eq. (9) will be satisfied:  $\eta_d = \eta_{\text{up}} = \eta_C$ , reflecting the enhancement of CIE efficiency through the information changes.

The first inequality in Eq. (9) reveals the second advantage of the CIE: Its efficiency is greater than or

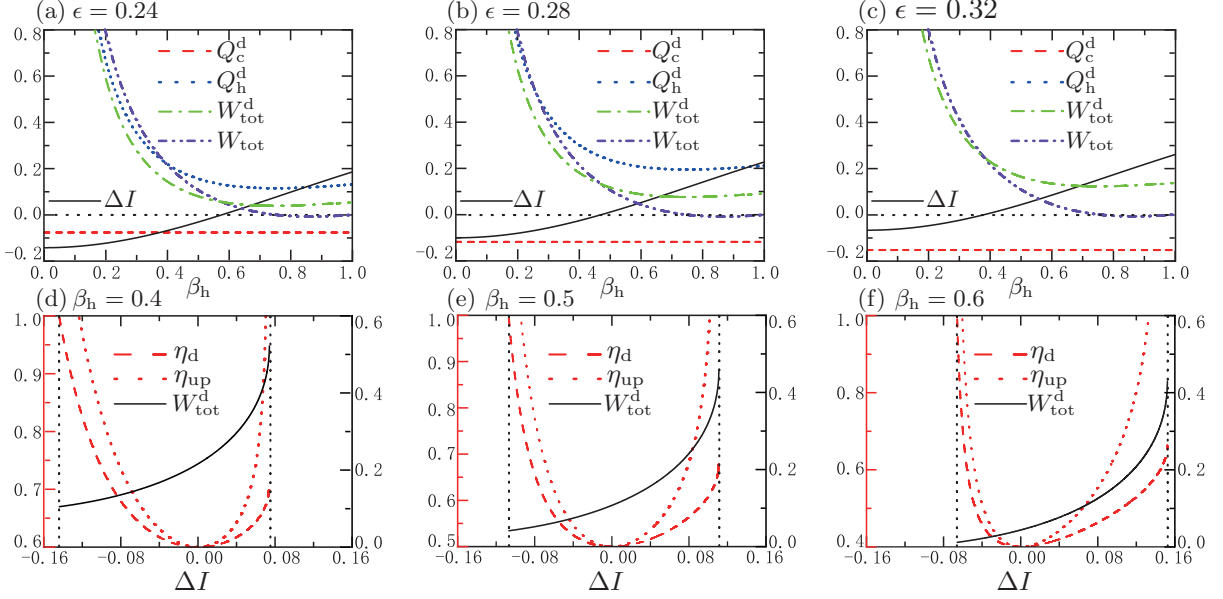


FIG. 2: Performance characteristics of the spin-1/2 CIE and the standard Carnot engine. The absorbed heat from the cold reservoir  $Q_c^d$ , the total input energy  $Q_h^d$ , the total output work  $W_{tot}^d$ , the information changes  $\Delta I$  in the spin-1/2 CIE, the output work  $W_{tot}$  in the standard Carnot engine as functions of the inverse hot temperature  $\beta_h$  for (a)  $\epsilon = 0.24$ , (b)  $\epsilon = 0.28$ , and (c)  $\epsilon = 0.32$ . The output work  $W_{tot}^d$ , the efficiency  $\eta_d$ , and the efficiency upper bound  $\eta_{up}$  as the functions of the information changes  $\Delta I$  for (d)  $\beta_h = 0.4$ , (e)  $\beta_h = 0.5$ , and (f)  $\beta_h = 0.6$ . The other parameters are  $\omega_A = 1.5$ ,  $\omega_C = 2$ ,  $\beta_c = 1$ , and  $n_e = -n_g = 1/2$ .

equal to than the standard Carnot due to the information changes. In Eqs. (5), the condition for the system to absorb zero heat from the cold reservoir is given by  $S_\epsilon = S_c$ , causing the third advantage of the CIE emerge. Under this condition, the information changes become to  $\Delta I = S_c - S_h$ . At this time, the total output work satisfies  $W_{tot}^d = Q_h^d = W_d - \Delta I/\beta_h \geq 0$ , meaning the CIE efficiency reaches 100%, which is forbidden for the standard Carnot engine.

*Numerical analysis for spin-1/2 Carnot information engine.*— To illustrate our ideas, we present a numerical analysis using a spin-1/2 CIE as depicted in Fig. 1(b), where the populations are distributed as  $n_e = -n_g = 1/2$ . Figs. 2(a)-(c) show that the CIE exhibits an extended operational regime compared to the standard Carnot engine. The numerical results demonstrate that the CIE can operate as a heat engine in the regime  $\beta_c \omega_A / \omega_C = 0.75 \leq \beta_h < \beta_c$ , for  $Q_c^d < 0$ ,  $Q_h^d > 0$ , and  $W_{tot}^d > 0$ . However, in this regime, the standard Carnot heat engine is thermodynamically forbidden, for  $W_{tot} < 0$ . This extension stems from two mechanisms: (a) the net work generated by information changes,  $W_{net}$ , offsets the negative work produced by the standard Carnot cycle, thereby enabling the CIE to perform positive work overall; (b) The dissipated heat  $\Delta I/\beta_c$  caused by the information changes counterbalance the positive heat  $Q_c$ , effectively resulting in a positive heat  $-Q_c^d$  flow into the cold reservoir. Moreover, Figs. 2(a)-(c) reveal that in the regime of positive information changes ( $\Delta I > 0$ ), where the net work  $W_{net} > 0$ , the CIE produces more work compared to the standard Carnot heat engine, consistent with Eq. (7). The efficiency  $\eta_d$  as a function of  $\beta_h$

please see Appendix D.

In Figs. 2(d)-(f), the red dashed curve, while consistently remaining above the Carnot efficiency (horizontal axis), lies below the red dotted curve, confirming Eq. (9). Additionally,  $\eta_d$  exhibits the same behavior as  $\eta_{up}$  with increasing  $\Delta I$ . In the regime  $\Delta I \leq 0$ ,  $\eta_d$  monotonically increases from the Carnot value  $\eta_C = 1$  when  $\Delta I$  reaches the minimum  $\Delta I = S_c - S_h$ . At this point, the CIE absorbs zero heat from the cold reservoir, enabling complete conversion of the input energy  $Q_h^d$  into output work. In the regime  $\Delta I \geq 0$ , the efficiency  $\eta_d$  increases monotonically with information changes until  $\Delta I$  reaches its maximum at  $\Delta I = \ln 2 - S_c$ . The analysis of this non-monotonic efficiency behavior with respect to the information changes is provided in Appendix E.

*Experimental scheme.*—The CIE can be implemented experimentally by a single trapped  $^{40}\text{Ca}^+$  ion, where the  $S_{1/2}$  and  $S_{-1/2}$  energy levels encode the system's states, while the ion's motional modes serve as the work storage. The total Hamiltonian of the ion [48, 49] consists of three components  $H = H_s + H_{har} + H_{int}$ , where  $H_s = \omega_s(t)\sigma_z/2 + \Omega_s\sigma_x/2$  represents the system spin Hamiltonian,  $H_{har} = \omega_{har}a^\dagger a$  describes the harmonic oscillator Hamiltonian used for work storage, and  $H_{int} = -(\tilde{\eta}\Omega_s/2)\sin(\omega_{har}t)\sigma_y$  serves as the interaction term. Here,  $\omega_s(t)$ ,  $\Omega_s$ ,  $\omega_{har}$ ,  $\tilde{\eta}$ ,  $\sigma_{x,y,z}$ , and  $a^\dagger$  ( $a$ ) denote the driving external field, the Rabi frequency of the driving external field, the oscillator frequency, the Lamb-Dicke parameter, the Pauli matrices, and the creation (annihilation) operators, respectively. The adiabatic strokes are achieved through slow modulation of

$\omega_s$  [50]. The isothermal strokes are implemented by discretizing it into  $N$  segments, combining adiabatic evolution and isochoric thermalization [51, 52]. Measurement and feedback control can be realized via two composite light fields, with system control based on fluorescence frequency detection. For more details, please see Appendix F.

*Conclusions.*—Based on the standard Carnot cycle, we have developed an CIE, driven by two thermal reservoirs and an information reservoir. We demonstrate that information changes enable the CIE to operate in thermodynamically forbidden regimes of the standard Carnot cycle, lead that the efficiency of the CIE is greater than or equal to the standard Carnot efficiency. Most significantly, the CIE can achieve 100% efficiency ( $\eta_d = 1$ ) with positive work output. To further confirm our theoretical

findings, we propose a spin-1/2 CIE as a practical example, and design an experimental scheme for implementing the spin-1/2 CIE based on a trapped  $^{40}\text{Ca}^+$  ion system. Our findings not only provide a theoretical framework for designing information-assisted heat engines that transcend conventional thermodynamic bounds, but also pave the way for the practical realization of dissipationless heat engines.

## Acknowledgments

Y. Xiao thanks the support in part by the National Natural Science Foundation of China Grant No. 21721003.

## Appendix A: The equations of the measurement and control strokes

At point  $C$ , following the measurement operation, the system-demon correlation is established. The mutual information between them is quantified as [53]

$$\begin{aligned}
I_C &= \sum_{x_C, y} P(y|x_C)P(x_C) \ln \frac{P(y|x_C)}{P(y)} \\
&= P(y=e|x_C=e)P(x_C=e) \ln \frac{P(y=e|x_C=e)}{P_y^e} + P(y=g|x_C=e)P(x_C=e) \ln \frac{P(y=g|x_C=e)}{P_y^g} \\
&+ P(y=e|x_C=g)P(x_C=g) \ln \frac{P(y=e|x_C=g)}{P_y^e} + P(y=g|x_C=g)P(x_C=g) \ln \frac{P(y=g|x_C=g)}{P_y^g} \\
&= (1-\epsilon) \ln(1-\epsilon) + \epsilon \ln \epsilon - [P_C^e(1-\epsilon) + P_C^g \epsilon] \ln P_y^e - [P_C^g(1-\epsilon) + P_C^e \epsilon] \ln P_y^g \\
&= S_Y - S_\epsilon,
\end{aligned} \tag{A1}$$

where,  $\epsilon = P(y \neq x_C|x_C)$  denotes the measurement error.  $P_C^e = P(x_C = e)$ , and  $P_C^g = P(x_C = g)$  represent the probabilities of the system being in excited state and ground state at point  $C$ , respectively. Here  $S_Y = -P_y^g \ln P_y^g - P_y^e \ln P_y^e$  represents the demon's entropy, with  $P_y^e = P(y=e) = P_C^e(1-\epsilon) + P_C^g \epsilon$  and  $P_y^g = P(y=g) = P_C^e \epsilon + P_C^g(1-\epsilon)$  being the probabilities of measurement outcomes  $e$  and  $g$ , respectively.  $S_\epsilon = -(1-\epsilon) \ln(1-\epsilon) - \epsilon \ln \epsilon$  denotes the entropy of the measurement error. Then, the demon utilizes this information to perform work to modulate the system's state, which makes the system state become to  $P_{C'}^e = P_C^e P(y=g|x_C=e) + P_C^g P(y=e|x_C=g) = \epsilon$  and  $P_{C'}^g = P_C^e P(y=e|x_C=e) + P_C^g P(y=g|x_C=g) = 1-\epsilon$ . Based on the distribution  $P_{C'}^e$  and  $P_{C'}^g$ , the work exerted by the demon on the system can be calculated as

$$\begin{aligned}
W_d &= \sum_{x_C, x_{C'}, y} P(x_C \rightarrow x_{C'}|y) P(y) (\varepsilon_{C'}^{x_{C'}} - \varepsilon_C^{x_C}) = \sum_{x_C, x_{C'}} P(x_C, x_{C'}) (\varepsilon_{C'}^{x_{C'}} - \varepsilon_C^{x_C}) \\
&= \sum_{x_{C'}} \sum_{x_C} P(x_C, x_{C'}) \varepsilon_{C'}^{x_{C'}} - \sum_{x_C} \sum_{x_{C'}} P(x_C, x_{C'}) \varepsilon_C^{x_C} = \sum_{x_{C'}} P(x_{C'}) \varepsilon_{C'}^{x_{C'}} - \sum_{x_C} P(x_C) \varepsilon_C^{x_C} \\
&= \omega_C [(P_{C'}^e n_e + P_{C'}^g n_g) - (P_C^e n_e + P_C^g n_g)],
\end{aligned} \tag{A2}$$

where  $P(x_C \rightarrow x_{C'}|y)$  is the condition probability for the system's evolutionary trajectory from  $x_C$  to  $x_{C'}$  based on the measurement outcome  $y$  which is equal to the condition probability  $P(x_C|y)$  due to this control stroke is

nondegenerate. After the first control stroke  $C \rightarrow C'$ , the residual mutual information takes the form:

$$\begin{aligned}
I_{C'} &= \sum_{x_{C'}, y} P(x_{C'}|y)P(y) \ln \frac{P(x_{C'}|y)}{P(x_{C'})} \\
&= P(x_{C'} = e|y = e)P_y^e \ln \frac{P(x_{C'} = e|y = e)}{P_{C'}^e} + P(x_{C'} = g|y = e)P_y^e \ln \frac{P(x_{C'} = g|y = e)}{P_{C'}^g} \\
&+ P(x_{C'} = e|y = g)P_y^g \ln \frac{P(x_{C'} = e|y = g)}{P_{C'}^e} + P(x_{C'} = g|y = g)P_y^g \ln \frac{P(x_{C'} = g|y = g)}{P_{C'}^g} \\
&= P(y = e|x_C = g)P_C^g \ln \frac{P(y = e|x_C = g)P_C^g}{P_y^e P_{C'}^e} + P(y = e|x_C = e)P_C^e \ln \frac{P(y = e|x_C = e)P_C^e}{P_y^e P_{C'}^g} \\
&+ P(y = g|x_C = e)P_C^e \ln \frac{P(y = g|x_C = e)P_C^e}{P_y^g P_{C'}^e} + P(y = g|x_C = g)P_C^g \ln \frac{P(y = g|x_C = g)P_C^g}{P_y^g P_{C'}^g} \\
&= P_C^e \ln P_C^e + P_C^g \ln P_C^g - [P_C^e(1 - \epsilon) + P_C^g \epsilon] \ln P_y^e - [P_C^g(1 - \epsilon) + P_C^e \epsilon] \ln P_y^g. \tag{A3}
\end{aligned}$$

Following [32, 47], through the stochastic entropy flows from the system, the heat absorbed from the cold reservoir during the third control stroke can be calculated as

$$\begin{aligned}
Q_c^d &= \sum_{x_{D'}, x_A, y} \beta_c^{-1} P(x_{D'} \rightarrow x_A|x_{D'}, y)P(x_{D'}|y)P(y) \ln \frac{P(x_A \rightarrow x_{D'}|x_A, y)}{P(x_{D'} \rightarrow x_A|x_{D'}, y)} \\
&= \beta_c^{-1} \sum_{x_{D'}, x_A, y} P(x_A)P(x_{D'}|y)P(y) \ln \frac{P(x_{D'})}{P(x_A)} \\
&= \beta_c^{-1} \sum_{x_A} P(x_A) \sum_{x_{D'}} \sum_y P(x_{D'}, y) \ln P(x_{D'}) - \beta_c^{-1} \sum_{x_{D'}, y} P(x_{D'}, y) \sum_{x_A} P(x_A) \ln P(x_A) \\
&= \beta_c^{-1} [\sum_{x_{D'}} P(x_{D'}) \ln P(x_{D'}) - \sum_{x_A} P(x_A) \ln P(x_A)] \\
&= \beta_c^{-1} (S_c - S_\epsilon), \tag{A4}
\end{aligned}$$

which is inequivalent to  $\beta_c^{-1} \langle \Delta S_{X|Y}^{D'A} \rangle$ . Here,  $\langle \Delta S_{X|Y}^{D'A} \rangle$  represents the average conditional entropy production along the trajectory  $x_{D'} \rightarrow x_A|y$ , given by

$$\begin{aligned}
\langle \Delta S_{X|Y}^{D'A} \rangle &= \sum_{x'_{D'}, x_A, y} P(x_{D'} \rightarrow A|y)P(y) \ln \frac{P(x_{D'}|y)}{P(x_A|y)} = \sum_{x'_{D'}, x_A, y} P(x_{D'}|y)P(y)P(x_A) \ln \frac{P(x_{D'}|y)}{P(x_A)} \\
&= \sum_{x'_{D'}, x_A, y} P(x_{D'}, y)P(x_A) \ln \frac{P(x_{D'}|y)}{P(x_A)} = \sum_{x'_{D'}, x_A, y} P(x_{D'}, y)P(x_A) [\ln \frac{P(x_{D'}|y)}{P(x_{D'})} + \ln \frac{P(x_{D'})}{P(x_A)}] \\
&= \sum_{x_A} P(x_A) \sum_{x'_{D'}, y} P(x_{D'}, y) \ln \frac{P(x_{D'}|y)}{P(x_{D'})} + \sum_{x_A} P(x_A) \sum_{x'_{D'}} \ln P(x_{D'}) \sum_y P(x_{D'}, y) \\
&- \sum_{x'_{D'}, y} P(x_{D'}, y) \sum_{x_A} P(x_A) \ln P(x_A) \\
&= \sum_{x'_{D'}, y} P(x_{D'}, y) \ln \frac{P(x_{D'}|y)}{P(x_{D'})} + \sum_{x'_{D'}} P(x_{D'}) \ln P(x_{D'}) - \sum_{x_A} P(x_A) \ln P(x_A) \\
&= S_c - S_\epsilon + I_{C'}, \tag{A5}
\end{aligned}$$

where we have used  $P(x_{D'} = e) = P(x_{C'} = e) = \epsilon$  and  $P(x_{D'} = g) = P(x_{C'} = g) = 1 - \epsilon$ . Here,  $S_c = -\sum_{x_A} P(x_A) \ln P(x_A) = -P_A^e \ln P_A^e - P_A^g \ln P_A^g$  denotes the system's entropy at point A, while  $S_\epsilon = -\sum_{x_{D'}} P(x_{D'}) \ln P(x_{D'}) = -\epsilon \ln \epsilon - (1 - \epsilon) \ln(1 - \epsilon)$  represents the entropy of the system at point  $D'$  which is also the entropy of measurement error. In Eq. (A4), the equivalence between the absorbed heat from the cold reservoir and

the product of the cold temperature and system's coarse-grained entropy change indicates reversible dynamics at the coarse-grained level for the composite system (system+reservoir). The total microscopic entropy production, including the system, the cold reservoir, and the demon, is defined as  $\sigma_{X|Y} = \Delta S_{X|Y}^D - \beta_c Q_c^d$  which satisfies  $\sigma_{X|Y} = I_{C'} \neq 0$ , revealing irreversible dynamics in the complete system (system+reservoir+demon) due to information dissipation [32].

### Appendix B: The definition of the CIE efficiency

We present some fundamental justifications for defining the efficiency of the Carnot information engine (CIE) as the ratio between the work output of the working system and the total energy investment. (i) Considering the definition where total output work comprises the demon-extracted work,  $-W_d$ , and working system producing,  $W_{\text{tot}}^d$ , which reads  $W = W_{\text{tot}}^d - W_d = Q_c^d + Q_h$  [12], the corresponding efficiency  $\eta = W/Q_h = \eta_C - \Delta I/(\beta_c Q_h)$  coincides with the upper bound derived for discrete quantum measurement and control [29] when  $I_{C'} = 0$ . Obviously, this efficiency can exceed the Carnot limit ( $\eta > \eta_C$ ) when  $\Delta I < 0$ . In the special case where  $Q_c^d = 0$ , we obtain  $W = Q_h \neq 0$ , achieving perfect efficiency  $\eta = 1$ . Thus, even under this definition, in our CIE the information changes still enable it to defeat the standard Carnot limit. (ii) The working system and the demon operate through fundamentally distinct mechanisms in work generation. The working system produces work through size changes, analogous to volume changes in the classical steam engines. In contrast, the demon extracts work by modifying the system's distribution—a qualitatively different process that alters the statistical properties rather than mechanical coordinates of the system. Therefore, combining the demon-extracted work and working system output work into a total work output lacks physical justification, for their fundamentally distinct operational mechanisms. (iii) The work done on the system by the demon  $W_d$  is used to change the distribution of the system with constant frequency, which is similar to inject equivalent heat into the system. Additionally, in Refs. [54, 55], the heat engine efficiency is defined as the ratio of the work produced by the working system to the total invested energy. The total invested energy consists of the passive thermal energy absorbed from the equilibrium reservoir and the ergotropy defined as the work required to transition the system from a passive to a non-passive state. Defining the total injection energy of the CIE as the sum of the absorbed heat from the hot reservoir and the work exerted by the demon is same as the total invested energy in Refs. [54, 55]. Thus, defining the CIE's efficiency as  $W_{\text{tot}}^d/(Q_h + W_d)$  is well-founded and physically justified. Furthermore, this definition, treating the demon's work as an energy investment rather than output, provides a more physically meaningful characterization of the engine's performance.

### Appendix C: The proof of the CIE efficiency bounds

Considering an isochoric process in which the system's frequency is held constant at  $\omega_C$ . The initial state distribution of the system mirrors the distribution observed at point  $C'$  ( $C$ ). Subsequently, the system interacts weakly with a thermal reservoir characterized by an inverse temperature  $\beta_h$  ( $\beta_d$ ). Over a sufficiently long time, this interaction drives the system into an equilibrium state corresponding to the distribution at point  $C$  ( $C'$ ). During this process, the heat absorbed by the system is  $-W_d$  ( $W_d$ ) and the associated entropy change is  $-\Delta I = S_h - S_\epsilon$  ( $\Delta I = S_\epsilon - S_h$ ). According to the second law of thermodynamics, the total entropy production satisfies  $S_h - S_\epsilon + \beta_h W_d \geq 0$  ( $S_\epsilon - S_h - \beta_d W_d \geq 0$ ), resulting the information changes and the work accompanying it satisfy  $\beta_h W_d \geq \Delta I$  ( $\Delta I \geq \beta_d W_d$ ).

### Appendix D: The CIE EFFICIENCY AS A FUNCTION OF THE Hot Inverse Temperature

Figs. 3(a)-(c) show that the efficiency of the CIE increases and then decreases as  $\beta_h$  increases. The reason for this trend can be explained as:

Based on Eqs. (1), (3), and (5) in the main text, the total output work of the CIE is derived

$$W_{\text{tot}}^d = (S_h - S_c) \left( \frac{1}{\beta_h} - \frac{1}{\beta_c} \right) + \omega_C (\langle n_d \rangle - \langle n_h \rangle) - \Delta I \beta_c^{-1}. \quad (\text{D1})$$

Taking the derivative of the output  $W_{\text{tot}}^d$  with the hot inverse temperature  $\beta_h$ , we derive

$$\left( W_{\text{tot}}^d \right)' = \frac{dW_{\text{tot}}^d}{d\beta_h} = \frac{[1+(1+\beta_h\omega_C)\exp(\beta_h\omega_C)]\ln P_C^e + \exp(\beta_h\omega_C)\{(\beta_h\omega_C)^2 + [1+\exp(\beta_h\omega_C) - \beta_h\omega_C]\ln P_C^g\}}{[1+\exp(\beta_h\omega_C)]^2} + S_c}{\beta_h^2}. \quad (\text{D2})$$

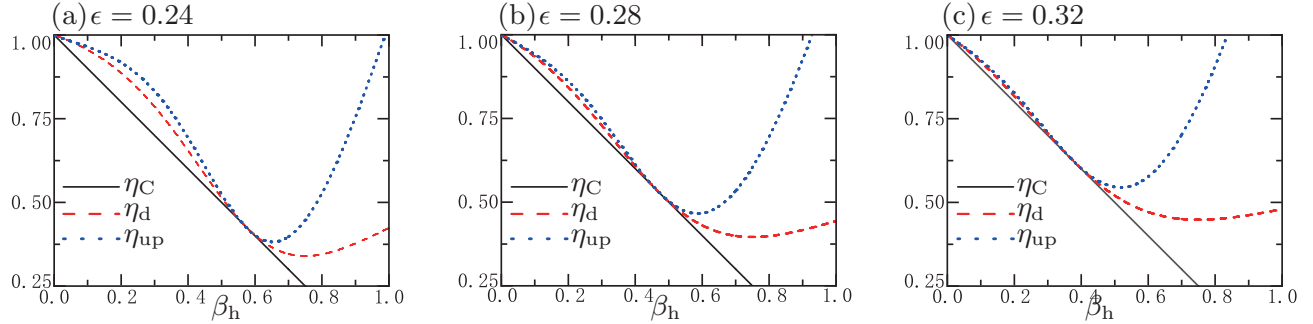


FIG. 3: The standard Carnot efficiency, the CIE efficiency  $\eta_d$ , and the upper bound of the CIE efficiency  $\eta_{\text{up}}$  as functions of the hot inverse temperature  $\beta_h$  for (a)  $\epsilon = 0.24$ , (b)  $\epsilon = 0.28$ , and (c)  $\epsilon = 0.32$ . The other parameters are  $\omega_A = 1.5$ ,  $\omega_C = 2$ ,  $\beta_c = 1$ , and  $n_e = -n_g = 1/2$

Given that  $\beta_h^2 > 0$ , the sign of the second fraction in Eq. (D2) depends on the numerator  $M_W$ . To analyze the behavior of  $M_W$  as a function of  $\beta_h$ , we differentiate it with respect to  $\beta_h$  and obtain

$$\frac{dM_W}{d\beta_h} = \frac{1}{4}\beta_h\omega_C^2\text{sech}^2\left(\frac{\beta_h\omega_C}{2}\right) > 0, \quad (\text{D3})$$

which reveals that  $M_W$  is an increasing function of  $\beta_h$ . Noting that, when  $\beta_h = \beta_c\omega_A/\omega_C$ ,  $M_W = 0$ . It follows that  $M_W \leq 0$  for  $0 < \beta_h \leq \beta_c\omega_A/\omega_C$ , and  $M_W > 0$  for  $\beta_c > \beta_h > \beta_c\omega_A/\omega_C$ , indicating that  $(W_{\text{tot}}^{\text{d}})'$   $\leq 0$  in the regime  $0 < \beta_h \leq \beta_c\omega_A/\omega_C$ , and  $(W_{\text{tot}}^{\text{d}})'$   $> 0$  in the regime  $\beta_c > \beta_h > \beta_c\omega_A/\omega_C$ . Consequently, the work  $W_{\text{tot}}^{\text{d}}$  in the regime  $0 < \beta_h < \beta_c\omega_A/\omega_C$  decreases and in the regime  $\beta_c > \beta_h > \beta_c\omega_A/\omega_C$  increases as  $\beta_h$  increases. According to Eq. (A4), the heat absorbed from the cold reservoir  $Q_c^{\text{d}} = (S_c - S_e)/\beta_c$  remains independent of  $\beta_h$ . Using the function  $W_{\text{tot}}^{\text{d}} = Q_c^{\text{d}} + Q_h^{\text{d}}$ , the efficiency Eq. (8) in main text can be written as  $\eta_d = W_{\text{tot}}^{\text{d}}/(W_{\text{tot}}^{\text{d}} - Q_c^{\text{d}})$ , indicating  $\eta_d$  is the monotonously increasing function of  $W_{\text{tot}}^{\text{d}}$  as long as  $Q_c^{\text{d}}$  is a constant. Thus, in Figs. 3(a)-(c), the efficiency  $\eta_d$  of the CIE has the same behavior as the work  $W_{\text{tot}}^{\text{d}}$ , initially decreasing and then increasing with  $\beta_h$ . At  $\beta_h = \beta_c\omega_A/\omega_C$ , where  $Q_h = 0$ , the efficiency  $\eta_d$  reaches its minimum value  $\eta_d = W_{\text{net}}/W_d$ , corresponding to the efficiency of the cycle  $C \rightarrow C' \rightarrow D' \rightarrow D \rightarrow C$  which is solely caused by the information changes.

Moreover, Figs. 3(a)-(c) demonstrate that when information changes vanish, where the demon fails to exploit information for entropy manipulation, the CIE's efficiency coincides with the standard Carnot efficiency. However, for non-zero information changes ( $\Delta I \neq 0$ ), regardless of whether the demon increases or reduces the system entropy, the CIE achieves higher efficiency than the Carnot limit, as predicted by Eq. (9) in the main text.

### Appendix E: The CIE EFFICIENCY AS A FUNCTION OF the Information changes

We now analyze how  $\eta_d$  varies with the information changes  $\Delta I$ . From the relation  $\langle \Delta n_d \rangle = (2\epsilon - 1)/2$ , the average population  $\langle n_d \rangle$  satisfy the relation  $-0.5 \leq \langle n_d \rangle \leq 0$ . We express the measurement error in terms of  $\langle n_d \rangle$  as  $\epsilon = (1 + 2\langle n_d \rangle)/2$ . Consequently, the measurement error entropy  $S_e$  takes the form  $S_e = -(1 + 2\langle n_d \rangle)/2 \ln[(1 + 2\langle n_d \rangle)/2] - (1 - 2\langle n_d \rangle)/2 \ln[(1 - 2\langle n_d \rangle)/2]$ , which increases as  $\langle n_d \rangle$  increases in the interval  $-0.5 \leq \langle n_d \rangle \leq 0$ . Since  $S_h$  remains independent of the  $\langle n_d \rangle$ , the information changes  $\Delta I = S_e - S_h$  also increase monotonically as  $\langle n_d \rangle$  increases.

According to Eq. (8) in main text, the derivative of  $\eta_d$  with respect to  $\langle n_d \rangle$  reads

$$\eta_d' = \frac{d\eta_d}{d\langle n_d \rangle} = \frac{\beta_h \{ \beta_h \omega_C [2 \ln 2 - 2S_c - \ln(1 - 2\langle n_d \rangle) - \ln(1 + 2\langle n_d \rangle)] - 4 \arctanh(2\langle n_d \rangle) (\beta_h \omega_C \langle n_h \rangle + S_c - S_h) \}}{2\beta_c [\beta_h \omega_C (\langle n_d \rangle - \langle n_h \rangle) + S_h - S_c]^2}. \quad (\text{E1})$$

For notational convenience, we denote the numerator in the right-hand side of Eq. (E1) as  $M_e$ . Given the positive denominator, the sign of Eq. (E1) is determined solely by  $M_e$ . To determine the sign of the numerator  $M_e$ , we calculate its derivative with respect to  $\langle n_d \rangle$  and obtain

$$\frac{dM_e}{d\langle n_d \rangle} = \frac{8\beta_h^2 [\omega_C (\langle n_d \rangle - \langle n_h \rangle) + (S_h - S_c)/\beta_h]}{1 - 4\langle n_d \rangle^2}. \quad (\text{E2})$$

Given the constraints  $-0.5 \leq \langle n_d \rangle \leq 0$  and  $\langle Q_h^{\text{d}} \rangle = \beta_h \omega_C (\langle n_d \rangle - \langle n_h \rangle) + (S_h - S_c)/\beta_h > 0$ , we find  $dM_e/d\langle n_d \rangle > 0$ , demonstrating that  $M_e$  monotonically increases with  $\langle n_d \rangle$  increases. Because when  $\langle n_d \rangle = \langle n_h \rangle$ ,  $M_e = 0$ , in the

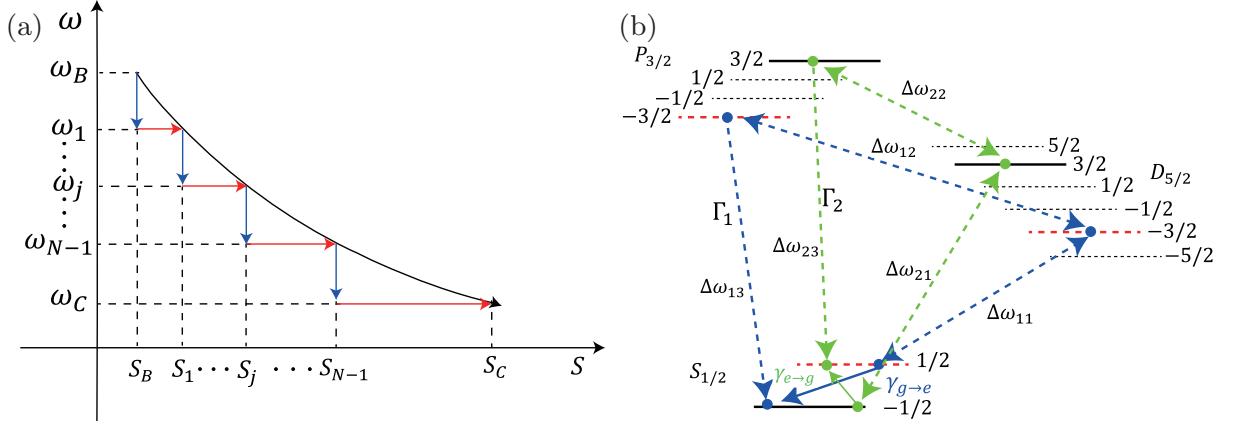


FIG. 4: (a) Schematic illustration for discretization of isothermal expansion process  $B \rightarrow C$ . Here the horizontal axis  $S$  denotes the system entropy and the vertical axis  $\omega$  represents the level spacing of the spin-1/2 system. (b) Schematic illustration of  $^{40}\text{Ca}^+$  energy level and energy transitions.

regime  $\langle n_d \rangle \leq \langle n_h \rangle$ ,  $M_e \leq 0$ , and in the regime  $\langle n_d \rangle > \langle n_h \rangle$ ,  $M_e > 0$ . These relations indicate that  $\eta'_d \leq 0$  in the regime  $\langle n_d \rangle \leq \langle n_h \rangle$ , and  $\eta'_d > 0$  in the regime  $\langle n_d \rangle > \langle n_h \rangle$ . So, in the regime  $\langle n_d \rangle \leq \langle n_h \rangle$ , the efficiency  $\eta_d$  increases as  $\langle n_d \rangle$  decreases, and in the regime  $\langle n_d \rangle > \langle n_h \rangle$ , the efficiency  $\eta_d$  increases as  $\langle n_d \rangle$  increases. Because the information changes  $\langle \Delta I \rangle$  also increase monotonically with  $\langle n_d \rangle$ , and  $\Delta I = 0$  when  $\langle n_d \rangle = \langle n_h \rangle$ , the information changes satisfy the relations: If  $\langle n_d \rangle \leq \langle n_h \rangle$ ,  $\Delta I \leq 0$ ; If  $\langle n_d \rangle > \langle n_h \rangle$ ,  $\Delta I > 0$ . Thus, the CIE efficiency decreases in the regime  $\Delta I < 0$ , but increase in the regime  $\Delta I \geq 0$  as the information changes increase.

### Appendix F: The EXPERIMENTAL SCHEME For The CIE

We implement our CIE using the electronic structure of a single trapped  $^{40}\text{Ca}^+$ . Specifically, we use the  $S_{1/2}$  and  $S_{-1/2}$  energy levels as the spin-up and spin-down states of the system. This spin system is coupled to a battery for work storage, realized through the quantized harmonic motion of the trapped ion. The total Hamiltonian of the composite system comprises three terms [48, 49]:  $H = H_s + H_{\text{har}} + H_{\text{int}}$ , where  $H_s = \omega_s(t)\sigma_z/2 + \Omega_s\sigma_x/2$  is the Hamiltonian of the system with Pauli matrices  $\sigma_{x,y,z}$ . Here,  $\omega_s(t)$  denotes a time-dependent driving field that enables precise manipulation of the system energy and  $\Omega_s$  represents the Rabi frequency of the driving field.  $H_{\text{har}} = \omega_{\text{har}}a^\dagger a$  represents the Hamiltonian of the battery where  $\omega_{\text{har}}$  is the oscillator frequency, and  $a^\dagger$  ( $a$ ) is the creation (annihilation) operator of the motional modes.  $H_{\text{int}} = -(\tilde{\eta}\Omega_s/2)\sin(\omega_{\text{har}}t)\sigma_y$  describes the system-battery interaction where  $\tilde{\eta}$  represents the Lamb-Dicke parameter.

The adiabatic compression stroke  $A \rightarrow B$  is implemented by applying a time-dependent external driving field over a duration  $\tau_{\text{ch}}$ . The field varies linearly according to the function  $\omega_s^{\text{ch}}(t) = \omega_A(1 - t/\tau_{\text{ch}}) + \omega_B t/\tau_{\text{ch}}$ , where  $0 \leq t \leq \tau_{\text{ch}}$ . During this process, the system Hamiltonian does not commute with itself at different times, leading to nonadiabatic transitions. The probability of the system transitioning from state  $|n\rangle$  to state  $|m\rangle$  is given by  $\xi = |\langle n|U_{\text{ch}}|m\rangle|^2$  [56] with unitary operator  $U_{\text{ch}} = \mathcal{T}_>\exp[-i\int_0^\tau dt H_{\text{ch}}(t)]$ , where  $\mathcal{T}_>$  is the time-ordering operator and  $H_s^{\text{ch}} = \omega_s^{\text{ch}}\sigma_z/2 + \Omega_s\sigma_x/2$ . If the system is driven slowly, the condition  $\xi \rightarrow 0$  will be satisfied, representing the quantum adiabatic theorem.

During the isothermal expansion stroke  $B \rightarrow C$ , the external field varies from  $\omega_B$  to  $\omega_C$ , while maintaining thermal equilibrium at inverse temperature  $\beta_h$ . To achieve this, we discretize this process into  $N$  sequential segments, each comprising an adiabatic evolution and an isochoric process [51, 52], as shown in Fig. 4(a). The field increment per segment is  $d\omega = (\omega_C - \omega_B)/N$ . For the  $j$ -th segment ( $j = 1, 2, 3, \dots, N$ ), the field evolves adiabatically as  $\omega_s^j(t) = \omega_{j-1}[1 - (t - t_{j-1})/(t_j - t_{j-1})] + \omega_j(t_j - t)/(t_j - t_{j-1})$ , where  $t_{j-1} \leq t \leq t_j$ , and  $\omega^j = \omega_B + jd\omega$  represents the field at the  $j$ -th isochoric process. In the isochoric process, the thermalization is achieved through a laser-induced cascade process, involving multiple electronic levels of the calcium ion. Specifically, to induce transitions from the excited (ground) state to the ground (excited) state, a laser with frequency  $\Delta\omega_{11}^j$  ( $\Delta\omega_{21}^j$ ) excites the electron from  $S_{1/2}$  ( $S_{-1/2}$ ) to  $D_{-3/2}$  ( $D_{3/2}$ ) followed by another laser with frequency  $\Delta\omega_{12}^j$  ( $\Delta\omega_{22}^j$ ), driving the transition from  $D_{-3/2}$  ( $D_{3/2}$ ) to  $P_{-3/2}$  ( $P_{3/2}$ ). Here,  $\Delta\omega_{11}^j, \Delta\omega_{12}^j, \Delta\omega_{21}^j$  and  $\Delta\omega_{22}^j$  correspond to the energy differences between  $S_{1/2}$  and  $D_{-3/2}$ ,  $D_{-3/2}$  and  $P_{-3/2}$ ,  $S_{-1/2}$  and  $D_{3/2}$ , and  $D_{3/2}$  and  $P_{3/2}$ . The electron then decays radiatively to  $S_{-1/2}$  ( $S_{1/2}$ ) with decay rate  $\Gamma_1$  ( $\Gamma_2$ ), as shown in Fig. 4(b). The effective transition rates from  $S_{1/2}$  to  $S_{-1/2}$  and from

$S_{-1/2}$  to  $S_{1/2}$  after these transitions are given by [57]

$$\gamma_{e \rightarrow g}^j = (\Omega_{11}^j)^2 \Gamma_1 / (\Omega_{12}^j)^2, \gamma_{g \rightarrow e}^j = (\Omega_{21}^j)^2 \Gamma_2 / (\Omega_{22}^j)^2, \quad (\text{F1})$$

where  $\Omega_{11}^j, \Omega_{12}^j, \Omega_{21}^j$ , and  $\Omega_{22}^j$  are the Rabi frequencies corresponding to the laser frequencies  $\Delta\omega_{11}^j, \Delta\omega_{12}^j, \Delta\omega_{21}^j$  and  $\Delta\omega_{22}^j$ , respectively. To ensure thermal equilibrium, the transition rates satisfy the detailed balance condition:  $\gamma_{e \rightarrow g}^j / \gamma_{g \rightarrow e}^j = P_{-1/2}^j / P_{1/2}^j = \exp(\beta_h \omega_j)$ . As  $N \rightarrow \infty$ , the segmented process approaches the ideal isothermal limit.

During the control stroke  $C \rightarrow C' \rightarrow D'$ , the measurement-based control employs two composite light fields:

$$\begin{aligned} E_g(t) &= \epsilon \cos(\Delta\omega_{21}^C t) + (1 - \epsilon) \cos(\Delta\omega_{13}^C t) \\ E_e(t) &= (1 - \epsilon) \cos(\Delta\omega_{11}^C t) + \epsilon \cos(\Delta\omega_{23}^C t). \end{aligned} \quad (\text{F2})$$

The frequency differences  $\Delta\omega_{11}^C, \Delta\omega_{21}^C, \Delta\omega_{13}^C$  and  $\Delta\omega_{23}^C$  correspond to the energy differences between the following electronic levels:  $S_{1/2}$  and  $D_{-3/2}$ ,  $S_{-1/2}$  and  $D_{3/2}$ ,  $S_{-1/2}$  and  $P_{-3/2}$ , and  $S_{1/2}$  and  $P_{3/2}$ , respectively. During the stroke  $C \rightarrow C'$ , the composite light fields  $E_g(t)$  or  $E_e(t)$  is used to measure whether the electron is in the ground or excited state. This field induces transitions between multiple electronic levels, enabling state detection through fluorescence measurements. The control protocol branches into four cases based on the detected photon frequency: (a) Detection of fluorescence at  $\Delta\omega_{21}^C$ : This indicates an incorrect measurement of the ground state ( $y = e$ ). A laser with frequency  $\Delta\omega_{21}^C$  is applied to excite the electron from  $S_{-1/2}$  to  $D_{3/2}$ , followed by another laser with frequency  $\Delta\omega_{22}^C$  to excite the electron from  $D_{3/2}$  to  $P_{3/2}$ . The electron then spontaneously decays to  $S_{1/2}$ , achieving a energy level inversion. This inversion operation takes time  $\tau_c$ . The system is then driven via the external field  $\omega_s^{\text{hc}}(t) = \omega_C(1 - t/\tau_{\text{hc}}) + \omega_{D'}t/\tau_{\text{hc}}$  to perform an adiabatic expansion from  $\omega_C$  to  $\omega_{D'}$ . Subsequently, the system is modulated back to its initial state, using the same procedure as the isothermal expansion stroke. (b) Detection of fluorescence at  $\Delta\omega_{13}^C$ : This indicates a correct measurement of the ground state ( $y = g$ ). After waiting for a time  $\tau_c$ , the system undergoes an adiabatic expansion and an isothermal compression same as case (a). (c) Detection of fluorescence at  $\Delta\omega_{11}^C$ : This indicates an correct measurement of the excited state ( $y = e$ ). A laser with frequency  $\Delta\omega_{11}^C$  is applied to excite the electron from  $S_{1/2}$  to  $D_{-3/2}$ , followed by another laser with frequency  $\Delta\omega_{12}^C$  to excite the electron from  $D_{-3/2}$  to  $P_{-3/2}$ . The electron then spontaneously decays to  $S_{-1/2}$ , achieving a energy level inversion. Then we perform the same operation as case (a) to the system. (d) Detection of fluorescence at  $\Delta\omega_{23}^C$ : This indicates a incorrect measurement of the excited state ( $y = g$ ). After waiting for a time  $\tau_c$ , the system undergoes an adiabatic expansion and an isothermal compression same as case (a).

To obtain the average values of work and heat, multiple process cycles are required. During each cycle, the fluorescence frequency, the change in the population of harmonic oscillator during the isothermal compression process, and the population changes after completing one cycle are recorded.

Next, the occurrences of each fluorescence frequency are counted and divided by the total number of cycles to determine the probability of each fluorescence. The corresponding heat absorbed from the cold and work for each fluorescence are then summed and divided by its occurrence count. This operation is used to calculate the average heat and work associated with that specific fluorescence.

Finally, the probability of each fluorescence occurrence is multiplied by its corresponding work and heat absorbed from the cold reservoir to obtain the average work and heat of the CIE after one complete cycle. Finally, the CIE efficiency can be determined by the equation:  $\eta_d = W_{\text{tot}}^d / (W_{\text{tot}}^d - Q_c^d)$ .

- |  |   |
|--|---|
| <p>[1] L. Szilard, über die entropieverminderung in einem thermodynamischen system bei eingriffen intelligenter, <i>Weissen. Z. Physik</i> <b>53</b>, 840-856 (1929).</p> <p>[2] T. Sagawa and M. Ueda, Generalized Jarzynski Equality under Nonequilibrium Feedback Control, <i>Phys. Rev. Lett.</i> <b>104</b>, 090602 (2010).</p> <p>[3] J. M. Horowitz and J. M. R. Parrondo, Designing optimal discrete-feedback thermodynamic engines, <i>New J. Phys.</i> <b>13</b>, 123019 (2019).</p> <p>[4] S. Yamamoto, S. Ito, N. Shiraishi, and T. Sagawa, Linear irreversible thermodynamics and Onsager reciprocity</p> | <p>for information-driven engines, <i>Phys. Rev. E</i> <b>94</b>, 052121 (2016).</p> <p>[5] L. Buffoni, A. Solfanelli, P. Verrucchi, A. Cuccoli, and M. Campisi, Quantum Measurement Cooling, <i>Phys. Rev. Lett.</i> <b>122</b>, 070603 (2019).</p> <p>[6] Z. Y. Lin, S. H. Su, J. Y. Chen, J. C. Chen, and J. F. G. Santos, Suppressing coherence effects in quantum-measurement-based engines, <i>Phys. Rev. A</i> <b>104</b>, 062210 (2021).</p> <p>[7] X. H. Ding, J. Y. Yi, Y. W. Kim, and P. Talkner, Measurement-driven single temperature engine, <i>Phys.</i></p> |
|--|---|

- Rev. E **98**, 042122 (2018).
- [8] J. Y. Yi, P. Talkner, and Y. W. Kim, Single-temperature quantum engine without feedback control, Phys. Rev. E **96**, 022108 (2017).
- [9] J. J. Park, K.H. Kim, T. Sagawa, and S. W. Kim, Heat Engine Driven by Purely Quantum Information, Phys. Rev. Lett. **111**, 230402 (2013)
- [10] C. Elouard, D. Herrera-Martí, B. Huard, and A. Auffèves, Extracting work from quantum measurement in Maxwell's demon engines, Phys. Rev. Lett. **118**, 260603 (2017).
- [11] C. Elouard and A. N. Jordan, Efficient quantum measurement engines, Phys. Rev. Lett. **120**, 260601 (2018).
- [12] P. Fadler, A. Friedenberger, and E. Lutz, Efficiency at Maximum Power of a Carnot Quantum Information Engine, Phys. Rev. Lett. **130**, 240401 (2023).
- [13] S. Seah, S. Nimmrichter, and V. Scarani, Maxwell's Lesser Demon: A Quantum Engine Driven by Pointer Measurements, Phys. Rev. Lett. **124**, 100603 (2020).
- [14] K. Chida, S. Desai, K. Nishiguchi, A. Fujiwara, Power generator driven by Maxwell's demon, Nat Commun **8**, 15301 (2017).
- [15] J. V. Koski, A. Kutvonen, I. M. Khaymovich, T. Ala-Nissila, and J. P. Pekola, On-Chip Maxwell's Demon as an Information-Powered Refrigerator, Phys. Rev. Lett. **115**, 260602 (2015).
- [16] L. Bresque, P. A. Camati, S. Rogers, K. Murch, A. N. Jordan, and A. Auffèves, Two-Qubit Engine Fueled by Entanglement and Local Measurements, Phys. Rev. Lett. **126**, 120605 (2021).
- [17] D. Mandal, H. T. Quan, and C. Jarzynski, Maxwell's Refrigerator: An Exactly Solvable Model, Phys. Rev. Lett. **111**, 030602 (2013).
- [18] D. Mandal and C. Jarzynski, Work and information processing in a solvable model of Maxwell's demon, Proc. Natl. Acad. Sci. U. S. A. **109**, 11641 (2012).
- [19] T. K. Saha, J. N. E. Lucero, J. Ehrich, D. A. Sivak, and J. Bechhoefer, Maximizing power and velocity of an information engine, Proc. Natl. Acad. Sci. U. S. A. **118**, e2023356118 (2021)
- [20] T. K. Saha, J. Ehrich, M. Gavrilov, S. Still, D. A. Sivak, and J. Bechhoefer, Information Engine in a Nonequilibrium Bath, Phys. Rev. Lett. **131**, 057101 (2023)
- [21] J. C. Maxwell, Theory of heat (Longmans London, 1871).
- [22] K. Maruyama, F. Nori, and V. Vedral, Colloquium: The physics of Maxwell's demon and information, Rev. Mod. Phys. **81**, 1 (2009).
- [23] E. Mizraji, The biological Maxwell's demons: exploring ideas about the information processing in biological systems. Theory Biosci. **140**, 307 (2021).
- [24] Y. Wen, Maxwell's demon at work: mitochondria, the organelles that convert in formation into energy? Chronic Dis. Transl. Med. **4**, 135 (2018).
- [25] M. Schirber, Information Flow in Molecular Machines, Physics **17**, 162 (2024).
- [26] S. Flatt, D. M. Busiello, S. Zamuner, and P. De Los Rios, ABC transporters are billion-year-old Maxwell Demons, Commun Phys **6**, 205 (2023).
- [27] V. Serreli, C. F. Lee, E. R. Kay, and D. A. Leigh, A molecular information ratchet, Nature **445**, 523 (2007).
- [28] T. Sagawa and M. Ueda, Fluctuation theorem with information exchange: role of correlations in stochastic thermodynamics, Phys. Rev. Lett. **109**, 180602 (2012).
- [29] T. Sagawa and M. Ueda, Second Law of Thermodynamics with Discrete Quantum Feedback Control, Phys. Rev. Lett. **100**, 080403 (2008).
- [30] G. Paneru, S. Dutta, T. Tlusty, and H. K. Pak, Reaching and violating thermodynamic uncertainty bounds in information engines, Phys. Rev. E **102**, 032126 (2020).
- [31] T. V. Vu and Y. Hasegawa, Uncertainty relation under information measurement and feedback control, J. Phys. A: Math. Theor. **53**, 075001 (2020).
- [32] Q. Zeng, J. Wang, New fluctuation theorems on Maxwell's demon, Sci. Adv. **7**, 23 (2021).
- [33] B. J. Lopez, N. J. Kuwada, E. M. Craig, B. R. Long, and H. Linke, Realization of a feedback controlled flashing ratchet, Phys. Rev. Lett. **101**, 220601 (2008).
- [34] S. Toyabe, T. Sagawa, M. Ueda, E. Muneyuki, and M. Sano, Experimental demonstration of information-to-energy conversion and validation of the generalized Jarzynski equality, Nat. Phys. **6**, 988 (2010).
- [35] G. Paneru, D. Y. Lee, T. Tlusty, and H. K. Pak, Lossless Brownian information engine, Phys. Rev. Lett. **120**, 020601 (2018).
- [36] Y. Jun, M. Gavrilov, and J. Bechhoefer, High-Precision Test of Landauer's Principle in a Feedback Trap, Phys. Rev. Lett. **113**, 190601 (2014).
- [37] J. V. Koski, V. F. Maisi, J. P. Pekola, and D. V. Averin, Experimental realization of a Szilard engine with a single electron, Proc. Natl. Acad. Sci. U. S. A. **111**, 13786 (2014).
- [38] J. V. Koski, V. F. Maisi, T. Sagawa, and J. P. Pekola, Experimental observation of the role of mutual information in the nonequilibrium dynamics of a Maxwell demon, Phys. Rev. Lett. **113**, 030601 (2014).
- [39] M. D. Vidrighin, O. Dahlsten, M. Barbieri, M. S. Kim, V. Vedral, and I. A. Walmsley, Photonic Maxwell's Demon, Phys. Rev. Lett. **116**, 050401 (2016).
- [40] N. Cottet, S. Jezouin, L. Bretheau, P. Campagne-Ibarcq, Q. Ficheux, J. Anders, A. Auffèves, R. Azouit, P. Rouchon, and B. Huard, Observing a quantum Maxwell demon at work, Proc. Natl. Acad. Sci. U. S. A. **114**, 7561 (2017).
- [41] S. Carnot, in Reflections on the Motive Power of Heat and on Machines Fitted to Develop that Power, edited by R. H. Thurston (Wiley, New York, 1890).
- [42] H. B. Callen, Thermodynamics and an Introduction to Thermostatistics (John Wiley & Sons, New York, 1985)
- [43] S. Deffner and C. Jarzynski, Information Processing and the Second Law of Thermodynamics: An Inclusive, Hamiltonian Approach, Phys. Rev. X, **3**, 041003 (2013).
- [44] S. Rana and A. M. Jayannavar, A multipurpose information engine that can go beyond the Carnot limit, J. Stat. Mech. (2016) 103207.
- [45] H. T. Quan, Y. X. Liu, C. P. Sun, and F. Nori, Quantum thermodynamic cycles and quantum heat engines, Phys. Rev. E **75**, 031105 (2007).
- [46] At point  $C'$ , the system state  $x_{C'}$  is determined by the system state  $x_C$  and the measurement outcome  $y$ . The post-control state  $x_{C'}$  can be expressed as a function of the state  $x_C$  and measurement outcome  $y$  following the relations:  $x_{C'}(x_C = e, y = e) = g$ ,  $x_{C'}(x_C = e, y = g) = e$ ,  $x_{C'}(x_C = g, y = e) = e$ ,  $x_{C'}(x_C = g, y = g) = g$ . In the cases  $x_{C'}(x_C = e, y = e) = g$  and  $x_{C'}(x_C = g, y = e) = e$  the demon injects work  $\varepsilon_C^g - \varepsilon_C^e = -\omega_C(n_e - n_g)$  and  $\varepsilon_C^e - \varepsilon_C^g = \omega_C(n_e - n_g)$  into the system. However, in the cases  $x_{C'}(x_C = e, y = g) = e$  and  $x_{C'}(x_C = g, y =$

- $g) = g$ , the demon performs zero work.
- [47] T. Schreiber, Measuring information transfer. *Phys. Rev. Lett.* **85**, 461 (2000).
- [48] W. E. Hou, X. Y. Zhao, K. Rehan, Y. Li, Y. Li, E. Lutz, Y. H. Lin, and J. F. Du, An energy efficient quantum-enhanced machine, arXiv:2404.15075.
- [49] O. V. Ivakhnenko, S. N. Shevchenko, and F. Nori, Nonadiabatic Landau-Zener-Stückelberg-Majorana transitions, dynamics, and interference, *Phys. Rep.* **995**, 1 (2023).
- [50] R. J. de Assis, T. M. de Mendonca, C. J. Villas-Boas, A. M. de Souza, R. S. Sarthour, I. S. Oliveira, and N. G. de Almeida, Efficiency of a quantum Otto heat engine operating under a reservoir at effective negative temperatures, *Phys. Rev. Lett.* **122**, 240602 (2019).
- [51] H. T. Quan, S. Yang, and C. P. Sun, Microscopic work distribution of small systems in quantum isothermal processes and the minimal work principle, *Phys. Rev. E* **78**, 021116 (2008).
- [52] E. Geva and R. Kosloff, A quantum-mechanical heat engine operating in finite time. A model consisting of spin-1/2 systems as the working fluid, *J. Chem. Phys.* **96**, 3054 (1992).
- [53] T. M. Cover, J. A. Thomas, *Elements of information theory* (Wiley, ed. 2, 2006).
- [54] W. Niedenzu, D. Gelbwaser-Klimovsky, A. G. Kofman, and G. Kurizki, On the operation of machines powered by quantum non-thermal baths, *New J. Phys.* **18**, 083012 (2016).
- [55] W. Niedenzu, V. Mukherjee, A. Ghosh, A. G. Kofman, and G. Kurizki, Quantum engine efficiency bound beyond the second law of thermodynamics, *Nat. Commun.* **9**, 165 (2018).
- [56] J. P. S. Peterson, T. B. Batalhão, M. Herrera, A. M. Souza, R. S. Sarthour, I. S. Oliveira, and R. M. Serra, Experimental characterization of a spin quantum heat engine, *Phys. Rev. Lett.* **123**, 240601 (2019).
- [57] L.-L. Yan, J.-W. Zhang, M.-R. Yun, J.-C. Li, G.-Y. Ding, J.-F. Wei, J.-T. Bu, B. Wang, L. Chen, S.-L. Su et al., Experimental verification of dissipation-time uncertainty relation, *Phys. Rev. Lett.* **128**, 050603 (2022).